ACS OMEGA

Open Access

http://pubs.acs.org/journal/acsodf

Article

pH-Responsive Amphiphilic Chitosan–Lignin System Loaded with Samarium Oxide Nanoparticles for Curcumin Delivery

Gilda Quezada, Floralba López, Paulina Romero, and Gema González*

Cite This: *ACS Omega* 2025, 10, 16138–16146

Read Online

ACCESS | Metrics & More | Article Recommendations | Supporting Information

ABSTRACT: Polymer nanoparticle-based drug carriers represent a new avenue for cancer therapy. In this work, we study the formation of chitosan/lignin (Chi/Lig) core–shell particles doped with samarium oxide nanoparticles as potential carriers for the hydrophobic anticancer drug curcumin. Electrostatic coassembly was responsible for the formation of Chi/Lig core–shell particles. The structural characterization suggested interactions between chitosan, lignin, and Sm_2O_3 through electrostatic interactions, such as hydrogen bonding. The incorporation of lignin into the chitosan matrix results in the formation of an amphiphilic core–shell structure, offering the potential for dual-drug-loading strategy studies, wherein one hydrophobic drug could reside in the lignin core while another hydrophilic drug occupies the chitosan shell. Additionally, the incorporation of lignin into the polymer systems not only contributes to a slower release of curcumin but also enables the design of pH-responsive drug carriers. Moreover, the strong red fluorescence observed in the samarium-containing composites suggests their potential for applications in bioimaging and in vitro assays, particularly with orally delivered microcarriers.

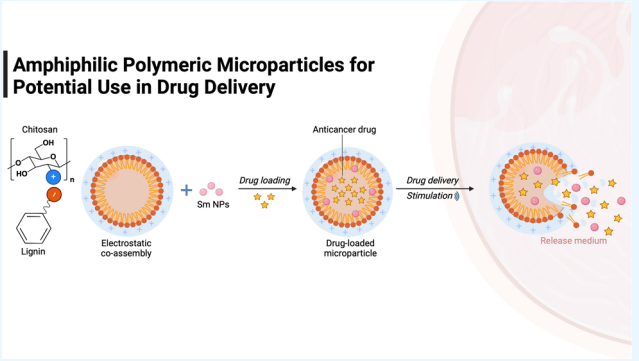

INTRODUCTION

Polymers have contributed significantly to the progress of drug delivery technology by facilitating the controlled release of therapeutic compounds at consistent doses over prolonged periods, enabling cyclical dosing, and offering tunable release profiles for hydrophilic and hydrophobic drugs.[1,2] The choice of polymer depends on its physical–chemical properties determined through extensive biochemical characterization and specific preclinical tests carried out to demonstrate its safety.[3] Medical advances have significantly influenced the design of new drug delivery systems, particularly smart polymers, which undergo physical or chemical transformations in response to external stimuli, offering advantages such as improved absorption rates, specific cell targeting, and sustained drug concentration within the therapeutic range.[4,5]

Exploration of natural anticancer drugs represents a promising strategy for less toxic cancer therapies. For example, curcumin, a low-cost, easily accessible, and low-toxic drug, is considered a promising chemopreventive agent by the US National Cancer Institute and has been under clinical investigation since the 1980s.[6] However, the pharmacological potential of curcumin is limited by its low absorption, photodegradation, and poor water solubility, resulting in low oral bioavailability and chemical stability.[6,7] Therefore, a delivery system is needed to address these limitations and improve the therapeutic efficacy of curcumin. It has been reported that polymer nanoparticles (NPs) improve curcumin absorption and water solubility, facilitating its metabolism and elimination through excretory pathways from the human body.[8] Furthermore, these nanoparticles can transport hydrophobic curcumin, improving its permeability and retention in the tumor microenvironment.[9]

Natural polymers, widely studied as vehicles for drug encapsulation and delivery, offer exceptional biocompatibility, controlled enzymatic degradation, specific biomolecule interactions, and ease of modification.[1,2] Cationic biopolymers with ionizable amine groups, such as chitosan, show promise in cancer therapy by deprotonating at pH 7.4 and protonating in mildly acidic environments, triggering drug release in tumor tissues.[5,10,11] The exhibited properties of chitosan in absorption enhancement,[12] controlled release,[13] tumor inhibition,[14] bioadhesive, and immune regulation[15,16] make it an excellent controlled release system. On the other hand, lignin, of which its antioxidant, antimicrobial,[17,18] antiviral[19] and anticoagulant properties[20] are known, make it a suitable system for applications in engineering tissues,[21] biocompatible antibacterial agents,[22] and drug delivery systems.[23]

Received: October 24, 2024
Revised: January 13, 2025
Accepted: January 23, 2025
Published: April 18, 2025

Lignin, being a negatively charged species, can be combined with positively charged chitosan to prepare composite polymer nanoparticles through electrostatic coassembly.[24] The combination of these biopolymers results in a multifunctional material with synergistically improved mechanical strength, stability, and functionality.[21,25] The antimicrobial properties of chitosan and the antioxidant properties of lignin make these compounds ideal for biocompatible and biodegradable drug delivery systems.[26] The use of chitosan/lignin composites aligns with the demand for sustainable drug delivery platforms, addressing environmental concerns.[27] These compounds hold great potential as scaffolds for tissue engineering, wound healing, and exhibit strong antibacterial and antimicrobial properties.[28−30]

Lignin/chitosan composites offer controlled release properties suitable for cancer therapy, ensuring sustained and targeted delivery of therapeutic agents.[29−32] For instance, lignin/chitosan nanoparticles were used to load hydrophilic cytarabine (Ara-C) and hydrophobic curcumin for release in a tumor environment,[32] reducing drug interactions. Chai et al. reported the synthesis of pH-responsive lignin/chitosan nanoparticles NPs to deliver anticancer drugs docetaxel (DTX) and curcumin (CUR),[31] showing good drug loading efficiency, biocompatibility, and pH-responsive release in tumor environments.[31] Furthermore, biocompatible luminescent nanoparticles, such as those doped with samarium, provide enhanced contrast for bioimaging, improving drug delivery applications.[33,34]

In this work, we investigate the behavior of pH-responsive drug delivery systems formed by electrostatic coassembly of chitosan/lignin core−shell particles doped with samarium oxide nanoparticles, as carriers for hydrophobic curcumin anticancer drugs. This opens new avenues for dual-drug-loading strategies and enhanced bioimaging applications, thereby contributing significantly to the field of targeted cancer therapy.

MATERIALS AND METHODS

Materials. Low molecular weight chitosan (95% deacetylated), acetic acid (CH_3COOH, 99%), sodium hydroxide (NaOH, 99%), alkali lignin (CAS No. 8068051), and samarium(III) nitrate hexahydrate ($Sm(NO_3)_3{\cdot}6H_2O$, 99.9%) were purchased from Sigma-Aldrich. Distilled water was used throughout the whole experiment. Curcumin was received as a yellow nanopowder from Haus Bioaceuticals Inc.

Preparation of Chi/Lig Microspheres. A 1% w/v chitosan solution in 1% acetic acid (at 580 rpm for 4 h at room temperature) and a 5% w/v lignin aqueous solution (at 370 rpm for 3 h) were prepared, resulting in solutions of pH 3.5 and pH 10, respectively. The chitosan−lignin (Chi/Lig) microspheres were prepared by mixing the chitosan and lignin solutions in a 10:1 v/v ratio, in a rotor−stator homogenizer for 5 min. From this colloidal suspension, films were prepared by the casting method, while Chi/Lig pellets were prepared by the dropwise addition of the colloidal suspension into a 1 M NaOH solution, which were collected, washed, dried, and lyophilized for 48 h. The films and pellets were properly stored for further characterization.

Synthesis of Sm_2O_3 NPs. The Sm_2O_3 NPs were synthesized by a precipitation method, adding drop by drop and under vigorous stirring, 250 mL of 1 M ammonium hydroxide into 50 mL of 0.1 M $Sm(NO_3)_3{\cdot}6H_2O$. A period of aging of 1 day at room temperature was needed for dehydration and further recrystallization. After centrifugation at 4000 rpm, the solid was washed with water and ethanol until neutral pH. The light yellow Sm_2O_3 powder obtained was dried at 90−120 °C for 3 h and calcined at 600 °C for 1 h.

Preparation of Chi/Lig/Sm Composite or Embedding of Polymer Material with Samaria Nanoparticles. Sm_2O_3 nanoparticles were incorporated into a 5% w/v lignin solution to prepare lignin/samarium (Lig/Sm) colloidal dispersions at concentrations 2, 5, and 8% w/v in samarium. These Lig/Sm dispersions were then mixed with a 1% chitosan solution in a 1:10 ratio and homogenized for 5 min. The resulting Chi/Lig/Sm dispersions (20, 50, and 80 ppm in Sm_2O_3 NPs) were used to prepare films and pellets of Chi/Lig/Sm, as indicated above by the casting method or dropwise adding into a 1 M NaOH solution, respectively.

Preparation of Chi/Lig/Sm−Cur NPs. A 0.1 ppm curcumin solution in 70% ethanol was prepared, assisted by sonication for 40 min. Then, in a 1:4 v/v ratio, this solution was mixed with a 5% lignin solution and allowed to dissolve for 10 min with intermittent vortexing. From the resulting Lig−Cur solution, a 40 ppm of Sm_2O_3 solution was prepared under sonication for 20 min and added to 1% chitosan to prepare a 2 mg/mL curcumin colloidal suspension, denoted as Chi/Lig/Sm−Cur, which was used to prepare Chi/Lig/Sm−Cur pellets by adding dropwise to a 1 M NaOH solution. It was determined that 1 mL of the Chi/Lig−Cur colloidal suspension (2 mg/mL curcumin) produces an average of 20 pellets, corresponding to an average of 0.1 mg of curcumin per pellet. The exact amount of loading is defined by the UV−vis calibration plot (Figure 1).

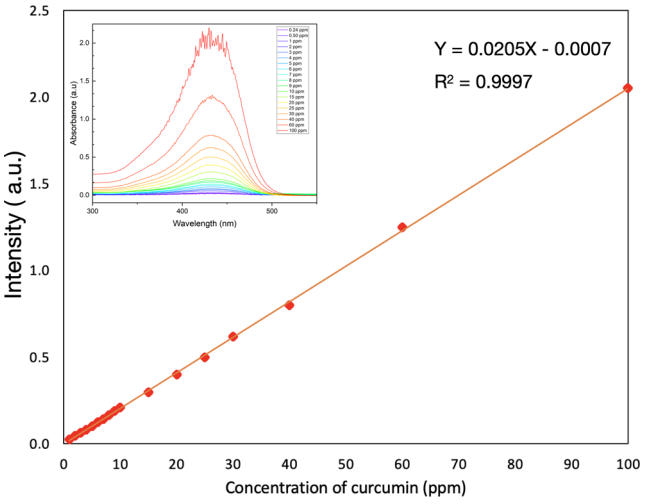

Figure 1. Calibration curve of curcumin obtained through UV−vis spectrophotometric analysis.

The pellets were collected, washed with distilled water, dried, and lyophilized for further characterization. For the Chi−Cur and Chi/Sm−Cur composites, the lignin incorporation step was omitted, while the Lig−Cur composite excluded the incorporation of chitosan.

Characterization of Chi/Lig, Chi/Lig/Sm, and Chi/Lig/Sm−Cur NPs. Microstructural analysis of the polymer systems was carried out using a TESCAN MIRA 3 SEM equipped with a Field-Emission Gun (FEG) Schottky electron emission source, operating at an acceleration voltage of 10 kV and was coupled with energy-dispersive X-ray microanalysis (EDS

https://doi.org/10.1021/acsomega.4c09697
ACS Omega 2025, 10, 16138−16146

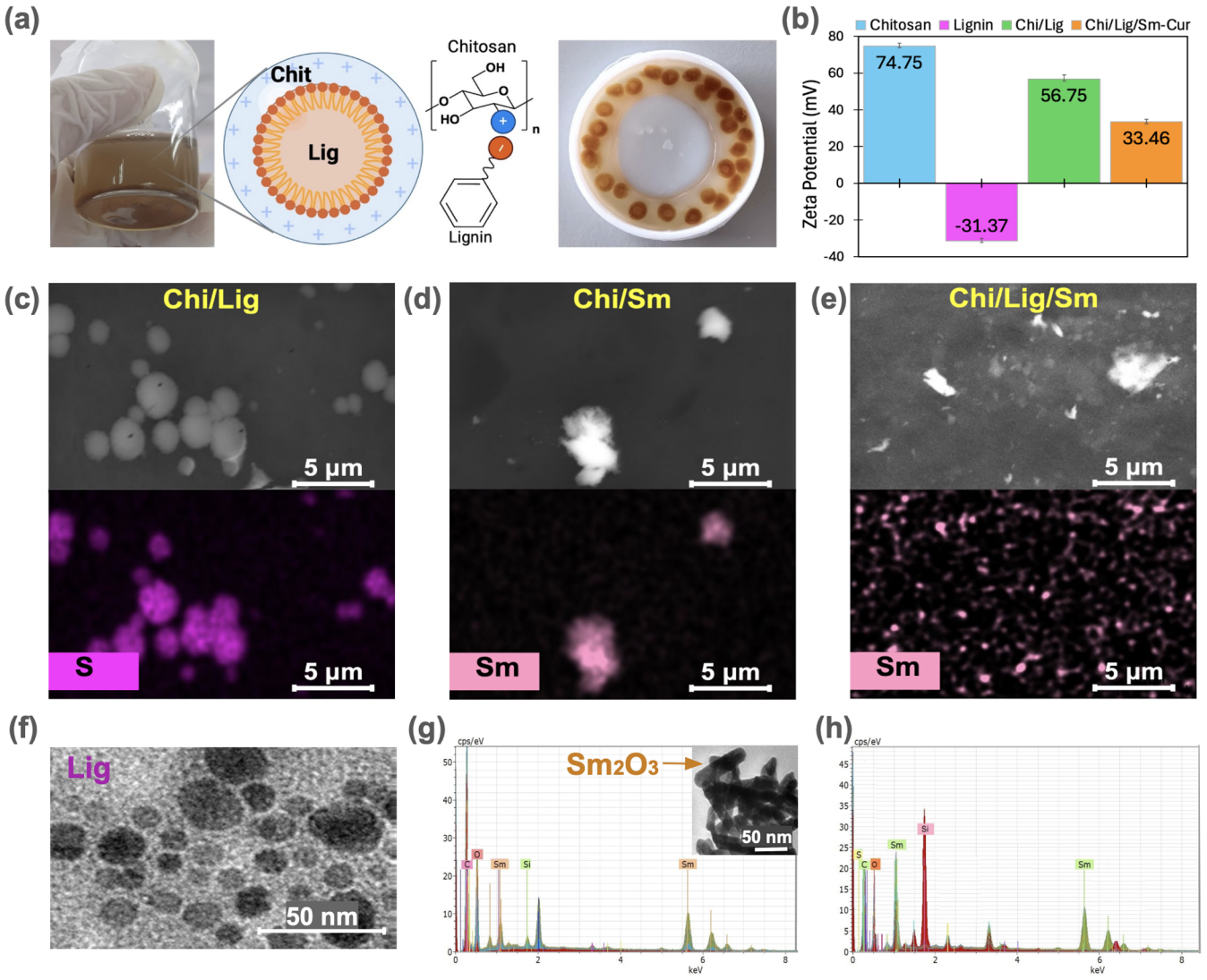

Figure 2. (a) Sketch of Chi/Lig microspheres formation by electrostatic coassembly. (b) ζ-potential of chitosan, lignin, and Chi/Lig solutions with error bars representing standard deviation. SEM-EDX elemental mapping analysis of (c) Chi/Lig, (d) Chi/Sm, and (e) Chi/Lig/Sm, (f) TEM of ligning NPs, (g) EDS of Chi/Sm sample; inset shows TEM of Sm_2O_3 Nps, and (h) EDS of Chi/Lig/Sm sample.

Bruker Quantax). Additionally, a Tecnai G20 Spirit Twin (FEI, NL) transmission electron microscope (TEM) at 80 kV was used to complement the microstructural analysis. Samples were dropped on Formvar-carbon 300× mesh grids, and excess water was removed by using a paper filter.

To evaluate the changes in the chemical structure of chitosan upon the incorporation of lignin, Sm_2O_3 NPs, and curcumin, Fourier-transform infrared (FTIR) spectroscopy was performed using an Agilent Cary 630 FTIR spectrometer equipped with a Diamond ATR accessory. Spectra were collected in the range of 4000−600 cm^{-1} with a resolution of 2 cm^{-1}. The crystalline structure of the synthesized Sm_2O_3 NPs was studied by a Rigaku MiniFlex, X-ray diffractometer for polycrystalline samples, equipped with a 600 W X-ray tube, Bragg−Brentano goniometer with 8-position autosampler, D/teX Ultra detector, and SmartLab Studio II software. Measurement conditions: X-ray generator operated at 40 kV and 15 mA, Cu Kα = 1.5418 radiation source (sealed tube), a $\theta/2\theta$ scanning axis was used for data collection, step width of 0.005°, 10−100° scan range in 2θ, 10°/min speed, and D/tex Ultra2 detector in one-dimensional (1D) scan mode.

Particle size and surface charge were determined by dynamic light scattering (DLS) and ζ-potential analysis using a NanoBrook 90Plus PALS particle size and ζ potential analyzer (Brookhaven Instruments Corp., NY). Optical characterization was performed using a UV−vis Spectrometer Model Lambda 1050 from PerkinElmer and a LEICA DM4000 LED microscope with a fluorescence lamp with a blue filter for (Ex: 340−380 nm, DC: 510 nm, EM: LP 515 nm) and an Olympus BX63 Motorized Upright.

Determination of Encapsulation Efficiency. Each one of the polymer systems loaded with curcumin was completely dispersed in an ethanol 0.1% aqueous solution, using an ultrasonic bath to achieve a uniform dispersion. For the quantification of encapsulated curcumin in the polymer system, a standard calibration curve was plotted by using standard concentrations of curcumin in 50% (v/v) ethanol. The changes in UV−vis absorbance of the solution at 432 nm were monitored by using a UV−vis spectrophotometer (SPECORD S600, Analytik Jena). The resulting calibration curve, with the respective spectra, is shown in Figure 1.

The encapsulation efficiency (EE) was calculated by

https://doi.org/10.1021/acsomega.4c09697
ACS Omega 2025, 10, 16138−16146

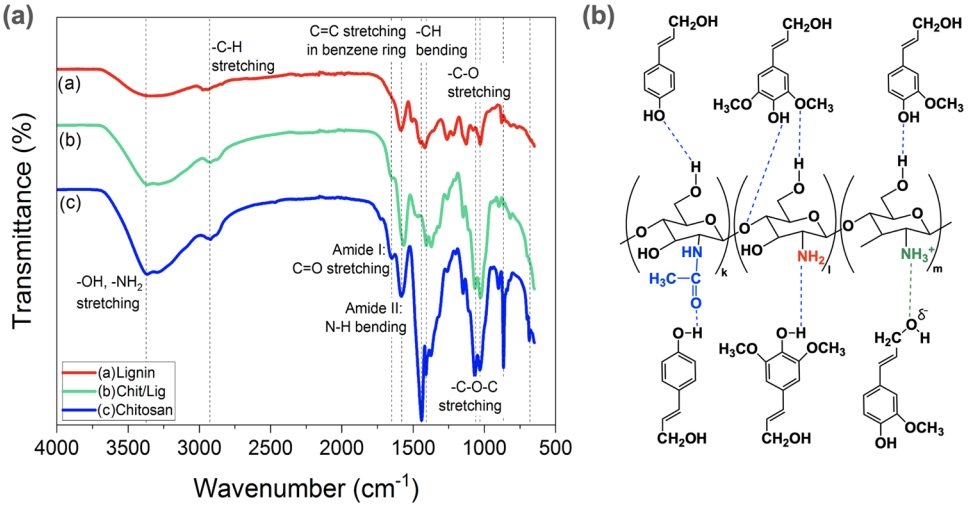

Figure 3. (a) FTIR spectra of lignin, chitosan/lignin (CHI/LIG), and chitosan. (b) Proposed scheme for hydrogen bond formation between the hydroxyl, amine, or carbonyl groups of chitosan and the hydroxyl and ether groups of lignin.

$$\text{EE}\ (\%) = \frac{[\text{CUR}]_{\text{pellet}}}{[\text{CUR}]_{\text{added}}} \times 100$$

were $[\text{CUR}]_{\text{added}}$ corresponds to the initial concentration of curcumin contained in the solution from which the pellets were loaded with curcumin at a concentration $[\text{CUR}]_{\text{pellet}}$.

In Vitro Release Assays. Curcumin-loaded polymer systems were suspended in a buffered solution at different pH conditions: simulated gastric fluid (SGF; pH 3) and simulated intestinal fluid (SIF; pH 7), stirred at 100 rpm at room temperature, and transferred into a dialysis bag with a molecular weight cutoff of 14 kDa. The curcumin is a conjugated system that absorbs in the visible range of 408−434 nm,[35−37] a property that enables its quantitative analysis using spectroscopic techniques. To monitor its release, aliquots of the supernatant were periodically extracted for UV−vis absorbance measurements at 432 nm, the wavelength corresponding to its maximum absorption. After measurement, the aliquots were returned to the original solution container to maintain consistent experimental conditions. This procedure was repeated until equilibrium was reached, ensuring a thorough analysis of each prepared polymer system.

The curcumin release kinetics was analyzed using different descriptive models, including zero-order, first-order, Higuchi, Korsmeyer−Peppas, and the Hixson−Crowell models.[38] These models were applied to evaluate the data obtained for the release studies.

RESULTS AND DISCUSSION

Pellets Formation and Morphology. The electrostatic coassembly between the positively charged amino groups of chitosan and the negatively charged carbonyl groups of lignin results in Chi/Lig microspheres. These microspheres present a micellar core composed of hydrophobic phenylalanine units, while hydrophilic hydroxyl and carboxyl groups form a micellar shell (Figure 2a).[39] Analysis of the ζ-potential for chitosan (+74.75 mV), lignin (−31.37 mV), and Chi/Lig microspheres (+56.75 mV) (Figure 2b) suggests that lignin is effectively encapsulated within the chitosan matrix. The reduced ζ-potential of Chi/Lig microspheres compared to pure chitosan indicates the formation of a stable colloidal suspension, with lignin contributing to stabilization via a double electrical layer, thereby preventing aggregation.[40] Furthermore, this stability is preserved when samarium oxide nanoparticles and curcumin are incorporated into the chitosan matrix, achieving an ζ-potential of 33.46 mV, a value indicative of good colloidal stability. The net cationic charge of Chi/Lig/Sm microspheres makes them potentially useful as drug carriers delivering hydrophobic, amphiphilic, or combined anticancer drugs such as curcumin.[21,26,30,31]

The morphologies of Chi/Lig, Chi/Sm, and Chi/Lig/Sm were characterized by using SEM, complemented by EDX for elemental mapping analysis (Figure 2c−e). The Chi/Lig sample reveals chitosan microspheres with diameters ranging from 2 to 6 μm, incorporating lignin nanoparticles with diameters 10−20 nm, as highlighted in the TEM micrograph in Figure 2f. Due to the sulfur content (1.5−1.9%) in the commercial alkali lignin used, elemental mapping of sulfur (S) allowed the identification of spherical lignin aggregates in the sample. The crystallite size of Sm_2O_3 NPs was determined by XRD with an average size of the 13 nm (Figure S1 in Supporting Information), which can be confirmed by TEM micrography in the inset of Figure 2g. The Sm_2O_3 incorporated into chitosan (Chi/Sm) leads to the aggregation of the samarium oxide NPs. This behavior can be attributed to the differing polar characteristics of the two components (Figure 2d). However, when lignin is added to the polymer system (Chi/Lig/Sm), samarium oxide nanoparticles are homogeneously distributed (Figure 2e) through the sample, avoiding the Sm_2O_3 NPs aggregates formation. The size of Chi/Lig/Sm pellets loaded with curcumin was estimated by DLS experiments (Figure S2 in Supporting Information), resulting in an effective diameter of 4574.3 nm with a polydispersity of 0.403. Although this size is rather large and unsuitable for intravenous injection, it can be used as orally deliver microcarriers and for in vitro bioimaging studies. On the other side, in order to reduce the microparticle size to achieve clinically relevant sizes (below 200 nm), the synthesis protocol can be optimized by adjusting the chitosan-to-lignin ratio or employing different synthesis methods. This would be important for the translational potential of the system.

FTIR Analysis. The interactions between chitosan and lignin are revealed in the FTIR spectra (Figure 3a) of lyophilized samples of chitosan, lignin, and Chi/Lig pellets.

https://doi.org/10.1021/acsomega.4c09697
ACS Omega 2025, 10, 16138−16146

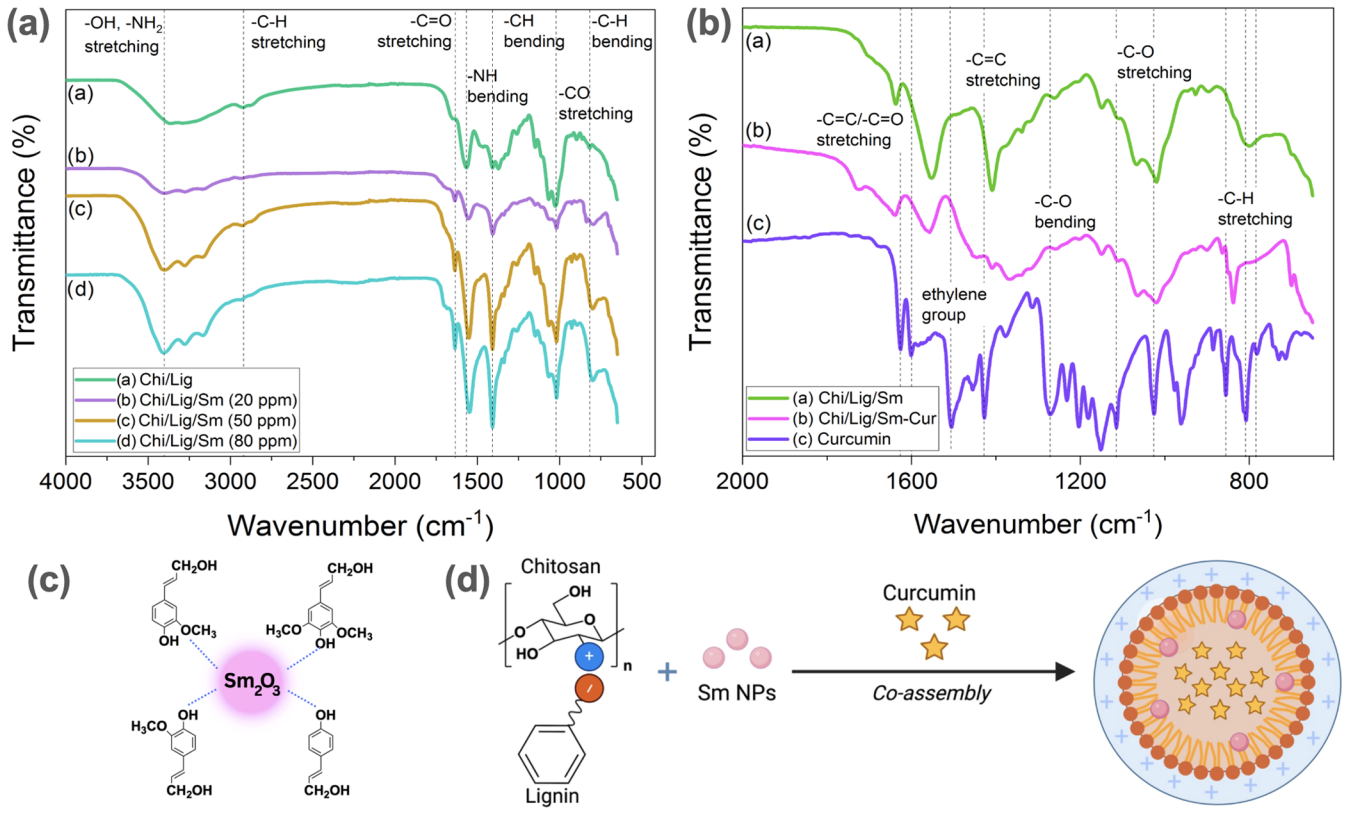

Figure 4. FTIR spectra of (a) Chi/Lig/Sm composites with varying incorporated concentrations of Sm_2O_3 nanoparticles and (b) Chi/Lig/Sm composite loaded with curcumin. (c) Proposed scheme for the interaction between Sm_2O_3 NPs and the hydroxyl groups in lignin units. (d) Sketch of formation of the Chi/Lig/Sm−Cur polymer system.

The lignin spectrum exhibits a characteristic broad band around 3365 cm^{-1}, associated with aromatic and aliphatic −OH groups, that along with the bands at 1451, 1418, and 1355 cm^{-1}, confirm that these O−H groups correspond to phenolic groups present in the lignin structure. Additionally, the peak at 2955 cm^{-1} corresponds to C−H stretching in aromatic, methoxy, and alkyl groups, while bands at 1583 and 1508 cm^{-1} are associated with C═C stretching in the phenolic groups of lignin. Furthermore, the bands at 1127 and 1028 cm^{-1} are linked to C−O stretching in aryl ether and ether groups, respectively, while the peak at 877 cm^{-1} represents an aromatic C−H out-of-plane deformation.

In the chitosan spectrum, a broad band between 3500 and 3100 cm^{-1} is observed, corresponding to −OH and $-NH_2$ stretching vibrations as well as intramolecular hydrogen bonding. The band at 2928 cm^{-1} is assigned to C−H stretching of the alkyl groups. The presence of residual N-acetyl groups is confirmed by the characteristic band at 1652 cm^{-1}, representing C═O stretching in amide I, while the peak at 1580 cm^{-1} arises from the N−H bending of primary amines. The band near 1440 cm^{-1} indicates $-CH_2$ bending, and the bands at 1067 and 1028 cm^{-1} correspond to C−O stretching, while the signal at 866 cm^{-1} is attributed to C−H out-of-plane bending in the monosaccharide ring.

The FTIR spectrum of the Chi/Lig composite shows similarities to that of pure chitosan with slight shifts and changes in peak intensities, indicating interactions with lignin. For instance, a decrease in the intensity of the OH band around 3000−3500 cm^{-1} is observed, which is also broader in the composite spectrum. Additionally, the peak at 1568 cm^{-1} is attributed to the overlap of N−H bending in chitosan and C═C stretching in the phenolic groups of lignin. The characteristic peak for $-CH_2$ bending in chitosan at around 1440 cm^{-1} is absent in the composite spectrum. These changes suggest the formation of hydrogen bonds between the hydroxyl, amine, or carbonyl groups of chitosan and the carbonyl, hydroxyl, or ether groups of lignin, as illustrated in the scheme in Figure 3b.

The incorporation of Sm_2O_3 nanoparticles into the Chi/Lig, resulting in a Chi/Lig/Sm composite, alters the chitosan−lignin interactions, freeing the amide and amine groups of chitosan. This is evident in Figure 4a, where the characteristic amine bands between 3000 and 3500 cm^{-1} become more defined as the concentration of samaria nanoparticles increases. This behavior is consistent with the enhanced intensity of the band at 1568 cm^{-1}, which corresponds to N−H bending as more samaria nanoparticles are incorporated into the composite. These observations suggest that Sm_2O_3 nanoparticles may be interacting with the −OH groups of both lignin and chitosan, as indicated by the reduction of OH signals in the composite. However, the distribution of Sm_2O_3 nanoparticles within the chitosan matrix (Figure 2d) and the Chi/Lig matrix (Figure 2e) points to a stronger affinity of the nanoparticles for lignin. The proposed interaction between samaria nanoparticles and lignin is illustrated in the scheme shown in Figure 4c.

FTIR spectra of Chi/Lig/Sm loaded with curcumin are shown in Figure 4b. The curcumin spectrum shows stretching vibrations at 1627 and 1603 cm^{-1} corresponding to the aromatic rings and predominantly to the overlapping stretching vibrations of alkenes (C ═ C) and carbonyl (C═O). Moreover, the peak at 1505 cm^{-1} indicates the presence of an ethylene group in curcumin. The peak of the C═C

https://doi.org/10.1021/acsomega.4c09697
ACS Omega 2025, 10, 16138−16146

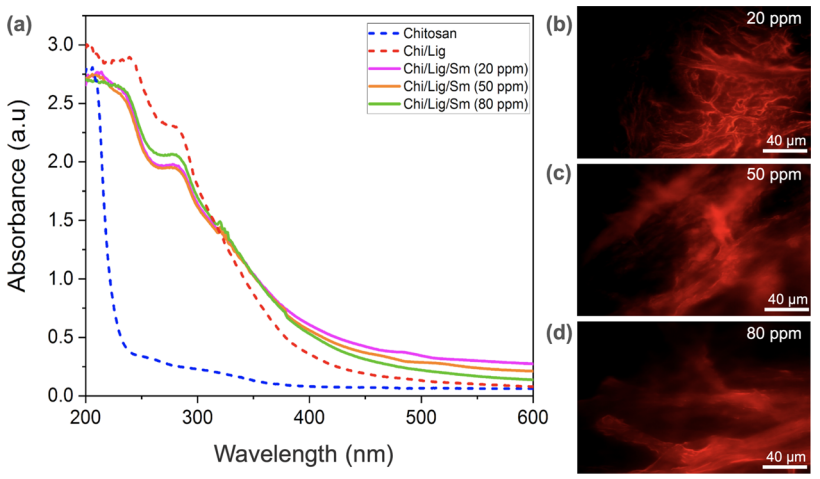

Figure 5. (a) UV−vis spectra of chitosan and Chi/Lig composite films with varying concentrations of Sm_2O_3 NPs. (b−d) Fluorescence micrographs of Chi/Lig composites doped with Sm_2O_3 NPs.

Table 1. Curcumin Encapsulation Efficiency (EE) and Release after 96 h Using Each of the Polymer Systems in SGF (pH = 3) and SIF (pH = 7)

				release (%)	
polymer system	$[Cur]_{added}$ (ppm)	$[Cur]_{pellet}$ (ppm)	EE (%)	SGF	SIF
Chi−Cur	80.0	10	12.5	78.8 ± 1.6	73.2 ± 0.6
Chi/Sm−Cur	80	14	17.5	79.0 ± 4.3	71.8 ± 0.9
Lig−Cur	160	74	46.3	33.6 ± 1.9	80.2 ± 0.2
Chi/Lig−Cur	80	38	47.5	55.0 ± 0.9	47.6 ± 0.8
Chi/Lig/Sm−Cur	80	32	40.0	65.0 ± 1.4	56.0 ± 0.7

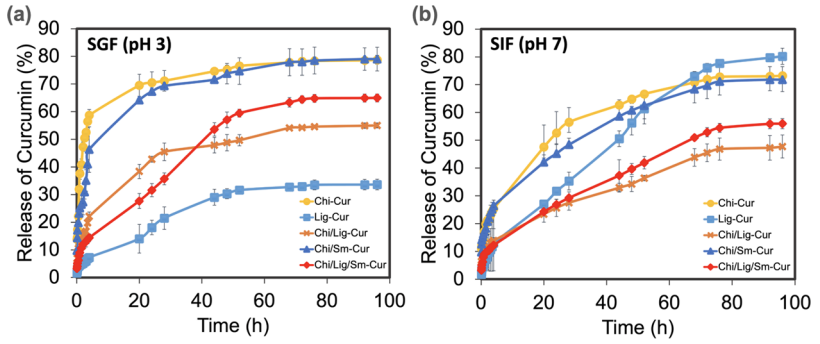

Figure 6. Release of curcumin during 96 h under (a) SGF and (b) SIF conditions from the different polymer systems tested: Chi−Cur, Lig−Cur, Chi/Lig−Cur, Chi/Sm−Cur, and Chi/Lig/Sm−Cur.

aromatic stretching vibration is located at 1427 cm^{-1}. Furthermore, a significant intense band at 1271 cm^{-1} is attributed to the bending vibration of the −CO phenolic band. The absorption peaks at 1140 and 1062 cm^{-1} correspond to the −CO stretching vibrations. The Chi/Lig/Sm−Cur spectrum is similar to that of Chi/Lig/Sm, with no noticeable peak differences. This suggests that the curcumin drug was effectively encapsulated within the pellets of Chi/Lig/Sm−Cur as shown in the scheme in Figure 4d.

Optical Characterization. UV−vis spectroscopy was performed on pristine chitosan and composite films (Chi/Lig and Chi/Lig/Sm) with different concentrations of Sm_2O_3 NPs (Figure 5a). The pristine chitosan, used as a control, did not exhibit any absorbance peaks at wavelengths above 200 nm, whereas the Chi/Lig spectrum shows two characteristic absorption peaks at 258 and 280 nm, which are attributed to the aromatic structure and the conjugated carbonyl group present in lignin. For all Chi/Lig/Sm containing Sm_2O_3 NPs, three distinct UV absorption peaks were observed in the 320−350 nm region. These peaks are attributed to electronic transitions between energy levels of the Sm^{3+} ions, specifically from the $4G_{5/2}$ excited state to various sublevels of the $6H_J$ ground state, where J represents the total angular momentum quantum number $\left(J = \frac{5}{2}, \frac{7}{2}, \frac{9}{2}, \frac{11}{2}, \frac{13}{2}, \frac{15}{2}\right)$. However, due to the relatively low concentration of Sm_2O_3 NPs in the Chi/Lig matrix, the intensity of those peaks is diminished by the strong absorbance of lignin. Figure 5b−d illustrates fluorescence microscopy images of Chi/Lig biopolymers doped with different concentrations of Sm_2O_3 NPs. The incorporation of samaria results in a pronounced red fluorescence, which might be useful for bioimaging applications.

Encapsulation Efficiency and Curcumin Release Assays. As can be seen in Table 1, both the chitosan (Chi−

https://doi.org/10.1021/acsomega.4c09697
ACS Omega 2025, 10, 16138−16146

Cur) and chitosan−samarium (Chi/Sm−Cur) samples loaded with curcumin exhibit the lowest encapsulation efficiency (EE), as well as a high release rate, under both pH (SFG and SIF) conditions. This behavior can be attributed to the weak affinity between curcumin and chitosan. In contrast, the incorporation of lignin into the polymer matrix significantly improves EE, with Lig−Cur, Chi/Lig−Cur, and Chi/Lig/Sm−Cur systems achieving EE values exceeding 40%, indicating a higher affinity between lignin and curcumin. Due to the molecular structures of lignin and curcumin, acidic conditions promote the attraction between them, affecting the release rate, as can be seen in Figure 6 and by comparing the release from chitosan matrices (Chi−Cur and Chi/Sm−Cur) with the release of those matrices containing lignin. Under SIF conditions, the electrostatic attraction between lignin and curcumin weakens, increasing the curcumin release. A likely mechanism for the capture of curcumin involves hydrogen bonding among the phenolic, carbonyl, and carboxyl groups of lignin and the hydroxyl groups of curcumin.

The addition of Sm_2O_3 nanoparticles to chitosan does not significantly affect the encapsulation or release of curcumin, suggesting a weak interaction between samaria and chitosan. However, when lignin is incorporated into the composite containing Sm_2O_3 NPs, the curcumin loading becomes slightly more challenging. This is due to the competing interactions between lignin−curcumin and lignin−samaria, which also contributes to an enhanced release of curcumin under both pH conditions evaluated.

The release of curcumin from the Chi/Lig−Cur composite is slightly increased in the presence of samarium under acidic pH conditions. In contrast, under SIF medium, the release of curcumin, initially lower, becomes higher than that in acid pH as Sm_2O_3 NPs are incorporated. This observation suggests that at SIF condition, the lignin−samaria interaction is favored, or alternatively, the lignin−curcumin interaction is weakened. Furthermore, since chitosan dissolves in acidic media, it is likely that under these conditions, the composite loses its chitosan "shell," exposing the micellar core where curcumin resides, thereby facilitating its release. These results are supported by the EDX micrographs shown in Figure 2d,e, which indicate a weak interaction between chitosan and samarium and a higher affinity for lignin and samaria.

The profiles shown in Figure 6a,6b correspond to the release of curcumin in SGF (pH 3) and SIF (pH 7) conditions, respectively, for the five polymer systems tested. The highest release percentages were exhibited for chitosan, both with (Chi/Sm−Cur) and without (Chi−Cur) samaria NPs, under SGF (pH 3) conditions. This behavior is consistent with the weak chemical interaction between chitosan and curcumin and the solubility of chitosan in acidic media. Under SIF conditions (pH 7), the release of curcumin from these systems was only slightly lower than in SGF, further indicating the weak interaction between chitosan and curcumin, and suggesting that the presence of samarium does not significantly impact the chitosan−curcumin interaction.

Incorporating lignin into the polymer systems, as seen in Chi/Lig−Cur and Chi/Lig/Sm−Cur, leads to a reduced curcumin release rate, indicating a stronger interaction between curcumin and lignin structures. This effect is further confirmed by examining the release of curcumin using the Lig−Cur polymer system, which shows the lowest release percentage under SGF conditions, suggesting efficient curcumin retention. Such control over the release of curcumin offers potential for developing sustainable systems with highly regulated drug delivery. Interestingly, the release of curcumin from Lig−Cur increases in SIF, likely due to the alkali nature of lignin, enhancing its solubility in the SIF medium. On the other hand, the other polymer systems exhibit lower release rates in SIF conditions, likely due to the greater solubility of chitosan in acidic media (SGF conditions). Under acidic conditions, the protonation of the amino groups of chitosan within the particle shell enhances electrostatic repulsion between polymer chains, potentially leading to the swelling of lignin−chitosan beads, thereby facilitating pH-responsive drug release.

A comparative analysis of the curcumin release behavior from the polymer systems evaluated in this study reveals strong agreement with previously reported findings.[29,31,39,41] For instance, Chai et al. investigated the synthesis of lignin−chitosan nanoparticles as pH-responsive carriers for anticancer agents, including docetaxel (DTX) and curcumin (CUR).[31] Their examination of curcumin release profiles under weakly acidic conditions showed a release rate of approximately 50% after 80 h.[31] This finding aligns with the 54% release rate after 80 h observed for the Chi/Lig−Cur system in the current study under simulated gastric fluid conditions (SGF pH 3). Moreover, the curcumin release behavior reported for Chai et al. was notably faster under weakly acidic conditions compared with physiologically normal pH (∼7), which aligns with the results obtained in this work. In addition, our results are consistent with other reports that study curcumin release from lignin nanoparticles.[41]

The curcumin release data from the Chi/Lig/Sm system were analyzed using the kinetic models listed in Table 2. In these models, C_o is the initial concentration of curcumin, while C_t denotes the amount of curcumin released at time t. The values of the regression coefficient (R^2), which indicate the goodness of fit for each model, are provided in Table 2 for both pH conditions. An R^2 value close to 1 suggests that the model best describes the release kinetics.

Table 2. Kinetic Analysis by Using Different Models for Curcumin Release from the Chi/Lig/Sum System in SGF (pH = 3) and SIF (pH = 7)

		R^2	
		SGF	SIF
zero-order model	$C_o - C_t = k_{ZO}t$	0.9261	0.9480
first-order model	$\ln\frac{C_o}{C_t} = k_{FO}t$	0.9531	0.9795
Korsmeyer−Peppas model	$\frac{C_t}{C_o} = k_{KP}t$	0.9909	0.9905
Higuchi model	$C_t = k_H\sqrt{t}$	0.9808	0.9976
Hixson−Crowell model	$C_o^{1/3} - C_t^{1/3} = k_{HC}t$	0.9456	0.9707

The Korsmeyer−Peppas and Higuchi models were identified as the most appropriate descriptions of curcumin release from the Chi/Lig/Sm system, as their R^2 values were close to 1 under both pH conditions tested. This indicates that the release process is complex and involves contributions from both diffusion and matrix relaxation mechanisms. However, the slight predominance of each model in sensitivity to pH suggests that the predominant release mechanism is influenced by the chemical environment. Furthermore, the exponent n for the Korsmeyer−Peppas model was calculated to be 0.47 at pH 3 and 0.52 at pH 7, indicating that curcumin release is

https://doi.org/10.1021/acsomega.4c09697
ACS Omega 2025, 10, 16138−16146

predominantly governed by diffusion through the polymeric matrix of the Chi/Lig/Sm system. This suggests that the concentration gradient serves as the primary driving force for the transport of curcumin to the external medium. The proximity of n to the critical value of 0.5[38,42−44] is the characteristic of systems where Fickian diffusion is the dominant mechanism, implying that other factors, such as polymer relaxation or swelling, exert minimal influence in this case.

CONCLUSIONS

The present study details the synthesis of a novel chitosan/lignin biopolymer doped with samarium for potential use in drug delivery. The formation of Chi/Lig microparticles occurred through electrostatic coassembly between the amino groups of chitosan and the carbonyl groups of lignin, forming a core−shell structure with lignin particles in the core and chitosan as the shell. In addition, coordinate bonds are formed between Sm_2O_3 NPs and chitosan molecules. The Chi/Lig/Sm system showed high red-intensity fluorescence, which might be useful for in situ bioimaging applications.

The Korsmeyer−Peppas and Higuchi models were identified as the most appropriate descriptions of the release of curcumin from the Chi/Lig/Sm system. However, the slight predominance of each model, depending on pH, suggests that the predominant release mechanism is influenced by the chemical environment. The versatile release behavior observed in different mediums highlights the potential of these polymeric systems for various drug delivery applications as they can be tailored to release drugs in specific manners to accommodate diverse needs, thus positioning them as promising candidates for drug delivery applications. This study contributes to the utilization of natural biopolymers in drug delivery applications and their potential application for encapsulating hydrophobic drugs. The examination of the release behavior of the Chi/Lig polymeric systems across mediums with varying pH levels reveals distinct release profiles, suggesting the potential for pH-responsive drug delivery systems. Furthermore, the incorporation of Sm_2O_3 NPs provides a follow-up environment through bioimaging for future studies. Understanding the assembly mechanisms and optical properties of our polymeric systems opens avenues for exploring controlled drug release and biosensing applications. While the current microparticles are relatively large and unsuitable for intravenous administration, they hold promise as oral delivery microcarriers and for in vitro bioimaging applications. To achieve clinically relevant sizes, the synthesis protocol could be refined by modifying the chitosan-to-lignin ratio or exploring alternative synthesis techniques. Such optimizations would enhance the system's translational potential.

ASSOCIATED CONTENT

Supporting Information

The Supporting Information is available free of charge at https://pubs.acs.org/doi/10.1021/acsomega.4c09697.

(PDF)

AUTHOR INFORMATION

Corresponding Author

Gema González − *School of Physical Sciences and Nanotechnology, Yachay Tech University, Urcuquí 100119, Ecuador; Centro de Ingeniería en Materiales y Nanotecnología, Instituto Venezolano de Investigaciones Científicas, Caracas 1020-A, Venezuela;* orcid.org/0000-0003-4526-2429; Email: ggonzalez@yachaytech.edu.ec

Authors

Gilda Quezada − *School of Physical Sciences and Nanotechnology, Yachay Tech University, Urcuquí 100119, Ecuador;* orcid.org/0009-0004-5843-5469

Floralba López − *School of Chemical Sciences and Engineering, Yachay Tech University, Urcuquí 100119, Ecuador*

Paulina Romero − *Laboratorio de Nuevos Materiales, Escuela Politécnica Nacional EPN, Quito 170525, Ecuador*

Complete contact information is available at: https://pubs.acs.org/10.1021/acsomega.4c09697

Notes

The authors declare no competing financial interest.

ACKNOWLEDGMENTS

The author would like to acknowledge the project: "Diseño de materiales nanoestructurados multifuncionales" (PHIS 23-06) of Yachay Tech University.

REFERENCES

(1) Liechty, W. B.; Kryscio, D. R.; Slaughter, B. V.; Peppas, N. A. Polymers for drug delivery systems. *Annu. Rev. Chem. Biomol. Eng.* **2010**, *1*, 149−173.

(2) Chandraprasad, M. S.; Dey, A.; Swamy, M. K. Introduction to Cancer and Treatment Approaches. In *Paclitaxel*; Academic Press, 2022; pp 1−27.

(3) Pillai, O.; Panchagnula, R. Polymers for drug delivery. *Curr. Opin. Chem. Biol.* **2001**, *5*, 447−451.

(4) Tong, X.; Pan, W.; Su, T.; Zhang, M.; Dong, W.; Qi, X. Recent advances in natural polymer-based drug delivery systems. *React. Funct. Polym.* **2020**, *148*, No. 104501.

(5) Agrawal, P. Significance of polymers in drug delivery system. *J. Pharmacovigilance* **2014**, *3*, No. e127.

(6) Baldi, A.; Luca, A. D.; Maiorano, P.; D'Angelo, C.; Giordano, A. Curcumin as an anticancer agent in malignant mesothelioma: A review. *Int. J. Mol. Sci.* **2020**, *21*, 1839.

(7) Ojo, O. A.; Adeyemo, T. R.; Rotimi, D.; Batiha, G. E.-S.; Mostafa-Hedeab, G.; Iyobhebhe, M. E.; Elebiyo, T. C.; et al. Anticancer properties of curcumin against colorectal cancer: a review. *Front. Oncol.* **2022**, *12*, No. 881641.

(8) Parveen, S.; Sahoo, S. K. Polymeric nanoparticles for cancer therapy. *J. Drug Targeting* **2008**, *16*, 108−123.

(9) Cho, K.; Wang, X. U.; Nie, S.; Chen, Z.; Shin, D. M. Therapeutic nanoparticles for drug delivery in cancer. *Clin. Cancer Res.* **2008**, *14*, 1310−1316.

(10) Hrubý, M.; Filippov, S. K.; Štěpánek, P. Smart polymers in drug delivery systems on crossroads: Which way deserves following? *Eur. Polym. J.* **2015**, *65*, 82−97.

(11) Masood, F. Polymeric nanoparticles for targeted drug delivery system for cancer therapy. *Mater. Sci. Eng., C* **2016**, *60*, 569−578.

(12) Ali, A.; Ahmed, S. A review on chitosan and its nanocomposites in drug delivery. *Int. J. Biol. Macromol.* **2018**, *109*, 273−286.

(13) Abdel-Aziz, H. M. M.; Hasaneen, M. N. A.; Omer, A. M. Nano chitosan-NPK fertilizer enhances the growth and productivity of wheat plants grown in sandy soil. *Span. J. Agric. Res.* **2016**, *14*, No. e0902.

(14) Xu, Y.; Wen, Z.; Xu, Z. Chitosan nanoparticles inhibit the growth of human hepatocellular carcinoma xenografts through an antiangiogenic mechanism. *Anticancer Res.* **2009**, *29*, 5103−5109.

(15) Kaneko, K.; Miyaji, E. N.; Gonçalves, V. M.; Ferreira, D. M.; Solórzano, C.; MacLoughlin, R.; Saleem, I. Evaluation of polymer

choice on immunogenicity of chitosan coated PLGA NPs with surface-adsorbed pneumococcal protein antigen PspA4Pro. *Int. J. Pharm.* **2021**, *599*, No. 120407.
(16) Rodrigues, S.; Dionísio, M.; Lopez, C. R.; Grenha, A. Biocompatibility of chitosan carriers with application in drug delivery. *J. Funct. Biomater.* **2012**, *3*, 615−641.
(17) Barapatre, A.; Meena, A. S.; Mekala, S.; Das, A.; Jha, H. In vitro evaluation of antioxidant and cytotoxic activities of lignin fractions extracted from Acacia nilotica. *Int. J. Biol. Macromol.* **2016**, *86*, 443−453.
(18) Espinoza-Acosta, J. L.; Torres-Chávez, P. I.; Ramírez-Wong, B.; López-Saiz, C. M.; Montaño-Leyva, B. Antioxidant, antimicrobial, and antimutagenic properties of technical lignins and their applications. *BioResources* **2016**, *11*, 5452−5481.
(19) Gordts, S. C.; Férir, G.; D'huys, T.; Petrova, M. I.; Lebeer, S.; Snoeck, R.; Andrei, G.; Schols, D. he low-cost compound lignosulfonic acid (LA) exhibits broad-spectrum anti-HIV and anti-HSV activity and has potential for microbicidal applications. *PLoS One* **2015**, *10*, No. e0131219.
(20) Mehta, A. Y.; Mohammed, B. M.; Martin, E. J.; Brophy, D. F.; Gailani, D.; Desai, U. R. Allosterism-based simultaneous, dual anticoagulant and antiplatelet action: allosteric inhibitor targeting the glycoprotein Iba-binding and heparin-binding site of thrombin. *J. Thromb. Haemostasis* **2016**, *14*, 828−838.
(21) Chen, L.; Tang, C.-y.; Ning, N.-y.; Wang, C.-y.; Fu, Q.; Zhang, Q. Preparation and properties of chitosan/lignin composite films. *Chin. J. Polym. Sci.* **2009**, *27*, 739−746.
(22) Morena, A. G.; Tzanov, T. Antibacterial lignin-based nanoparticles and their use in composite materials. *Nanoscale Adv.* **2022**, *4*, 4447−4469.
(23) Chowdhury, M. A. The controlled release of bioactive compounds from lignin and lignin-based biopolymer matrices. *Int. J. Biol. Macromol.* **2014**, *65*, 136−147.
(24) Liu, J.; Huang, Y.; Kumar, A.; Tan, A.; Jin, S.; Mozhi, A.; Liang, X.-J. pH-sensitive nano-systems for drug delivery in cancer therapy. *Biotechnol. Adv.* **2014**, *32*, 693−710.
(25) Zou, Z.; Ismail, B. B.; Zhang, X.; Yang, Z.; Liu, D.; Guo, M. Improving barrier and antibacterial properties of chitosan composite films by incorporating lignin nanoparticles and acylated soy protein isolate nanogel. *Food Hydrocolloids* **2023**, *134*, No. 108091.
(26) Zou, T.; Sipponen, M. H.; Österberg, M. Natural shape-retaining microcapsules with shells made of chitosan-coated colloidal lignin particles. *Front. Chem.* **2019**, *7*, No. 370.
(27) Naskar, S.; Kuotsu, K.; Sharma, S. Chitosan-based nanoparticles as drug delivery systems: a review on two decades of research. *J. Drug Targeting* **2019**, *27*, 379−393.
(28) Ravishankar, K.; Venkatesan, M.; Desingh, R. P.; Mahalingam, A.; Sadhasivam, B.; Subramaniyam, R.; Dhamodharan, R. Biocompatible hydrogels of chitosan-alkali lignin for potential wound healing applications. *Mater. Sci. Eng., C* **2019**, *102*, 447−457.
(29) Li, Y.; Peng, Y.; Hu, Y.; Liu, J.; Yuan, T.; Zhou, W.; Dong, X.; Wang, C.; Binks, B. P.; Yang, Z. Fabrication of poly (e-caprolactone)-embedded lignin-chitosan nanocomposite porous scaffolds from pickering emulsions. *Langmuir* **2023**, *39*, 6947−6956.
(30) Pothal, P.; Pathania, K.; Kumar, S.; Kaur, J.; Sah, S. P.; Singh, R.; Pawar, S. V. Lignin-chitosan biocomposite film for antimicrobial activity: Fabrication, characterization and in-vitro evaluation. *Mater. Lett.* **2023**, *337*, No. 133956.
(31) Chai, Y.; Wang, Y.; Li, B.; Qi, W.; Su, R.; He, Z. Microfluidic synthesis of lignin/chitosan nanoparticles for the pH-responsive delivery of anticancer drugs. *Langmuir* **2021**, *37*, 7219−7226.
(32) Chen, K.; Qian, Y.; Wang, C.; Yang, D.; Qiu, X.; Binks, B. P. Tumor microenvironment-responsive, high internal phase Pickering emulsions stabilized by lignin/chitosan oligosaccharide particles for synergistic cancer therapy. *J. Colloid Interface Sci.* **2021**, *591*, 352−362.
(33) Azlan, M. N.; Halimah, M. K.; Hajer, S. S.; Suraini, A. B.; Azlina, Y.; Umar, S. A. Enhanced optical performance of tellurite glass doped with samarium nanoparticles for fiber optics application. *Chalcogenide Lett.* **2019**, *16*, 215−229.
(34) Srinivasan, R.; Yogamalar, R.; Vinu, A.; Ariga, K.; Bose, A. C. Structural and optical characterization of samarium doped yttrium oxide nanoparticles. *J. Nanosci. Nanotechnol.* **2009**, *9*, 6747−6752.
(35) Priyadarsini, K. I. Photophysics, photochemistry and photobiology of curcumin: Studies from organic solutions, bio-mimetics and living cells. *J. Photochem. Photobiol., C* **2009**, *10*, 81−95.
(36) Nelson, K. M.; Dahlin, J. L.; Bisson, J.; Graham, J.; Pauli, G. F.; Walters, M. A. The essential medicinal chemistry of curcumin: miniperspective. *J. Med. Chem.* **2017**, *60*, 1620−1637.
(37) Kotha, R. R.; Luthria, D. L. Curcumin: biological, pharmaceutical, nutraceutical, and analytical aspects. *Molecules* **2019**, *24*, 2930.
(38) Nair, R. S.; Morris, A.; Billa, N.; Leong, C.-O. An evaluation of curcumin-encapsulated chitosan nanoparticles for transdermal delivery. *AAPS PharmSciTech* **2019**, *20*, No. 69.
(39) Azadfar, M.; Hiscox, W. C.; Chen, S. Solubilization of lignin in copolymer micelles in aqueous solution. *Colloids Surf., A* **2016**, *503*, 1−10.
(40) Gigli, V.; Capecchi, E.; Tortolini, C.; Isidori, A.; Antiochia, R.; Saladino, R. Tuning the Effect of Chitosan on the Electrochemical Responsiveness of Lignin Nanoparticles. *ACS Biomater. Sci. Eng.* **2023**, *9*, 3597−3605.
(41) Alqahtani, M. S.; Alqahtani, A.; Al-Thabit, A.; Roni, M.; Syed, R. Novel lignin nanoparticles for oral drug delivery. *J. Mater. Chem. B* **2019**, *7*, 4461−4473.
(42) Askarizadeh, M.; Esfandiari, N.; Honarvar, B.; Sajadian, S. A.; Azdarpour, A. Kinetic modeling to explain the release of medicine from drug delivery systems. *ChemBioEng Rev.* **2023**, *10*, 1006−1049.
(43) Gooneh-Farahani, S.; Naghib, S. M.; Naimi-Jamal, M. R. A novel and inexpensive method based on modified ionic gelation for pH-responsive controlled drug release of homogeneously distributed chitosan nanoparticles with a high encapsulation efficiency. *Fibers Polym.* **2020**, *21*, 1917−1926.
(44) Wang, R.; Shou, D.; Lv, O.; Kong, Y.; Deng, L.; Shen, J. pH-Controlled drug delivery with hybrid aerogel of chitosan, carboxymethyl cellulose and graphene oxide as the carrier. *Int. J. Biol. Macromol.* **2017**, *103*, 248−253.

https://doi.org/10.1021/acsomega.4c09697
ACS Omega 2025, 10, 16138−16146